Topological Braiding of Non-Abelian Midgap Defects in Classical Metamaterials

Yafis Barlas[1,2] and Emil Prodan[1]
[1]Department of Physics, Yeshiva University, New York, New York 10016, USA
[2]Department of Physics, University of Nevada Reno, Reno, Nevada 89522, USA

(Received 6 May 2019; revised manuscript received 23 September 2019; accepted 18 March 2020; published 7 April 2020)

Nontrivial braid-group representations appear as non-Abelian quantum statistics of emergent Majorana zero modes in one- and two-dimensional topological superconductors. Here, we generate such representations with topologically protected domain-wall modes in a classical analog of the Kitaev superconducting chain, with a particle-holelike symmetry and a $\mathbb{Z}_2$ topological invariant. The midgap modes are found to exhibit distinct fusion channels and rich non-Abelian braiding properties, which are investigated using a T-junction setup. We employ the adiabatic theorem to explicitly calculate the braiding matrices for one and two pairs of these midgap topological defects.

DOI: 10.1103/PhysRevLett.124.146801

An important characteristic of a topological insulator is the emergence of boundary electron states, whenever a sample is halved. Similar topological effects can be engineered in classical metamaterials, where spectral gaps at finite frequencies support wave-guiding modes along domains or boundaries. This topological behavior has been demonstrated with photonic [1–3], phononic [4–6], and mechanical [7–11] platforms. The electronic topological phases in condensed matter systems are classified by generic symmetries [12–15] and this classification also includes topological superconductors supporting Majorana quasiparticles as boundary modes [16,17]. These boundary modes are far more exotic as they display non-Abelian braiding and statistics [16,18,19]. While several classes of topological insulating systems have been implemented in metamaterials, the analog of topological superconducting systems has not been yet realized. As such, an important question remained open, namely, whether topologically degenerate resonant levels can be engineered in metamaterials and if these degenerate modes can be manipulated by adiabatic deformations which ultimately result in nontrivial representations of the braid group.

In this Letter, we answer this question in the affirmative by designing a one-dimensional (1D) metamaterial that exhibits nontrivial representations of the braid group. Regardless of the quantum or classical setting, the critical ingredients for these representations are the adiabatic theorem, a nontrivial configuration space, and a degenerate manifold of periodic solutions. We create them using the algorithmic map [20], which translates any strong topological condensed matter system along with its corresponding symmetries, to an absolutely equivalent topological metamaterial, built exclusively with passive components (such as magnetically coupled spinners [21]). The result is a classical analog of the particle-hole (PH) symmetric Kitaev chain [16], where topological midgap resonant modes can be stabilized by domain walls (DW) interpolating between trivial and topological regions. Since these modes are pinned at a fixed frequency and can be controlled by adiabatic displacements of DWs, one has the unique opportunity to explore the braiding of these point topological defects.

Our proposal is aided by two purely classical features with no quantum analogs, namely, the possibility to create two distinct DW configurations and the ability to control the "superconducting order parameter." As a result, in our model, the number of different domain wall configurations resulting in N midgap modes equals $2^{N/2}$ (see [22] for the counting argument). Additionally, we discovered two distinct fusion channels, with the same fusion rules as Ising anyons. Aimed with these similarities, we describe how a braiding cycle can be implemented with a T-junction geometry, similar to Ref. [18]. We show that, even though the equations of motion are quadratic in time, the braiding matrices can be computed using the adiabatic theorem [25]. This allows us to demonstrate, via explicit numerical calculations, that distinct exchange matrices result for different fusion channels. Using analytic arguments, based on the PH symmetry of the system and localization of the midgap modes, we demonstrate that the braids are independent of the details of the implementation, hence topological, as long as the DWs are kept sufficiently far apart. Furthermore, we construct unitary representations of the braid group [22], consistent with our numerical results.

Before we proceed, let us emphasize that in 1D topological superconductors (D-class systems), Majorana zero-mode braiding requires adiabatic deformations that break all accidental symmetries, particularly, the time-reversal symmetry [22]. As such, this task cannot be accomplished within the BDI class, for which mechanical analogs already exist [11]. Furthermore, in 1D systems, the $\mathbb{Z}_2$ (as opposed to $\mathbb{Z}$) stability is essential for implementing exchange for a

sequence of four Majorana zero modes [22], hence this task cannot be accomplished in the AIII class either. Note that exchanging just two Majorana zero modes presents no challenge and it has been implemented with 1D classical chiral symmetric wires (class AIII) [26]. As such, the $\mathbb{Z}_2$ PH-symmetric D-class setting is not a convenient choice but rather a necessity, and this is the challenge for metamaterial implementation which is addressed here. In two dimensions or in synthetic dimensions, non-Abelian geometric phases can be generated with other topological classes [27,28].

The classical analog of a fully general PH-symmetric Kitaev chain is shown in Fig. 1. If we encode the degrees of freedom in the vector $\mathbf{Q} = \{q_n^\alpha\}$, the collective motion is determined by the quadratic Lagrangian:

$$\mathcal{L} = \frac{1}{2}(\dot{\boldsymbol{Q}}^\dagger \dot{\boldsymbol{Q}} + \boldsymbol{Q}^\dagger D \boldsymbol{Q}), \quad \boldsymbol{Q}^\dagger D \boldsymbol{Q} = \sum_{n,\alpha;m,\beta} d_{nm}^{\alpha\beta} q_n^\alpha q_m^\beta, \tag{1}$$

written in appropriate units, and the equation of motion becomes $\ddot{\mathbf{Q}} = -D\mathbf{Q}$. With the labelings and couplings from Fig. 1, which were supplied by the map [20],

$$D = H + \omega_0^2 \mathbb{I}, \qquad H = -\tau_2 \otimes K, \tag{2}$$

where ω_0 is the pulsation of the uncoupled resonators, τ_2's is the off-diagonal Pauli matrix which couples the collective indices (1,2) with (3,4) (see Fig. 1 for details), and K is the Kitaev Hamiltonian [16]:

$$K = \frac{\imath}{2}(\Delta_x \sigma_1 + \Delta_y \sigma_3) \otimes (S - S^\dagger) - \hat{\sigma}_2 \otimes \left(\mu - \frac{t}{2}(S + S^\dagger)\right), \tag{3}$$

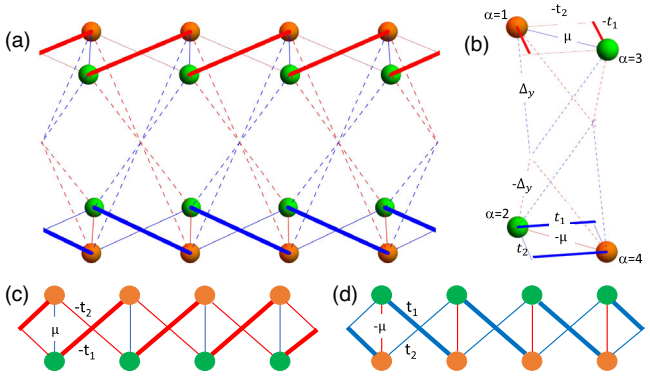

FIG. 1. (a) One-dimensional lattice with four identical resonators per unit cell. The resonators inside the nth cell are labeled by (n, α), with $\alpha = \overline{1,4}$. The connections between the resonators represent the real valued couplings $d_{nm}^{\alpha,\beta}$ in Eq. (1), with $t_1 = t + \Delta_x$ and $t_2 = t - \Delta_x$. The positive (negative) signs of the couplings are color coded in blue (red). (b) Detailed hopping pattern in the unit cell, viewed from a different angle. (c),(d) Top and bottom layers, respectively, which are coupled Su-Schrieffer-Heeger ladders (see text for more details).

with complex order parameter $\Delta = \Delta_x + \imath\Delta_y$, on-site chemical potential μ and hopping parameter t (fixed at 1). The shift operator of the lattice acts as $S\{q_n^\alpha\} = \{q_{n+1}^\alpha\}$ and σ_i's are the Pauli matrices which separately act on indices (1,2) and (3,4). The PH symmetry of (3) is implemented by the complex conjugation $\mathcal{C}$, which remains a symmetry even if the parameters Δ, μ are given site dependencies, e.g., to create domain walls.

All entries in D are real valued, as it should be for passive metamaterials, but this comes at the expense of doubling the Kitaev model. Nevertheless, note the intrinsic symmetry $[H, S_y] = 0$, with $S_y = -i\hat{\sigma}_2 \otimes \mathbb{I}$ ($S_y^2 = -\mathbb{I}$), which fully decouples the two copies. Indeed, if

$$\Pi_\pm = \frac{1}{2}(\mathbb{I} \mp \imath S_y) = \pi_\pm \otimes \mathbb{I}, \quad \pi_\pm = \frac{1}{2}\begin{pmatrix} 1 & \mp\imath \\ \pm\imath & 1 \end{pmatrix} \tag{4}$$

are the projections onto the symmetry sectors of S_y, then

$$H = H_+ \oplus H_-, \qquad H_\pm = \Pi_\pm H \Pi_\pm = \pi_\pm \otimes K. \tag{5}$$

Furthermore, each reduced Hamiltonian $H_\pm$ obeys PH symmetry $\Theta_{\mathrm{PH}} H_\pm \Theta_{\mathrm{PH}}^{-1} = -H_\pm$, with $\Theta_{\mathrm{PH}} = (\tau_1 \otimes \mathbb{I})\mathcal{C}$. The $\Pi_\pm$ sectors remain invariant under the dynamics, hence the mechanical system can be driven exclusively in one sector or the other [29]. As such, from now on, we concentrate exclusively on $D_+ = H_+ + \omega_0^2 \Pi_+$, which apart from a shift, is unitarily equivalent with K from (3). Note that the time-reversal operation maps one sector into the other, hence D_+ is not constrained by this symmetry and this is why we can implement the T-junction cycle.

The mapping procedure of Ref. [20] provides a fairly complex hopping pattern, which would be hard to guess at the onset. The effective PH symmetry acts on the internal degrees of freedom of the lattice and, to gain more intuition, we start by separating the top and bottom layers by setting $\Delta_y = 0$. The resulting top and bottom chains, with alternating t_1 and t_2 hopping patterns [see Figs. 1(c) and 1(d)], are a classical analog of coupled Su-Schrieffer-Heeger models, with pairs of green/orange resonators supplying effective spin degrees of freedom. The coupling μ provides an effective spin-orbit coupling, hence, in the limit of zero interlayer coupling, our model is the classical analog of a spin-orbit coupled wire. The interlayer coupling Δ_y connects the same type of sites in opposite layers, and represents the classical analog of the s-wave superconducting order parameter [30]. Hence, Fig. 1 represents the classical analog of two Kitaev chains [31], as argued above. The intrinsic symmetry of the lattice $[H, S_y] = 0$, acts on the top and bottom layers and represents a $\pi/2$ rotation in the internal effective spinor space. It fully decouples the two Kitaev chains.

The dispersion equation for a translational invariant configuration is $\omega_\pm^2(k) = \omega_0^2 \pm \sqrt{(\mu - t\cos k)^2 + |\Delta|^2 \sin^2 k}$, hence the spectrum of D_+ is symmetric relative to ω_0^2 and

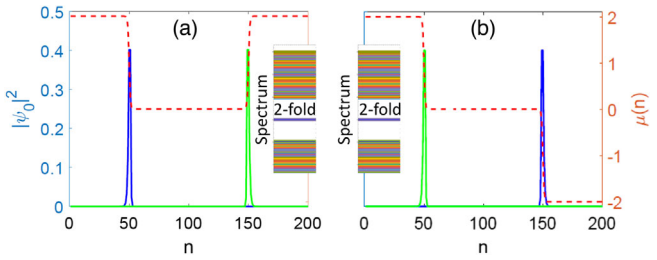

FIG. 2. (a) The $(++)$ domain wall configuration, generated by a spatial variation of μ (red-dashed line), interpolating between trivial ($\mu = 2$) and topological ($\mu = 0$) phases. The phase interfaces trap two midgap modes, whose amplitudes are shown in blue and green. The inset displays the spectrum of H_+ calculated with this domain wall configuration. (b) Same as (a) but for the $(+-)$ domain wall configuration.

displays a gap as long as $\mu \neq |t|$. The system is in a topological (trivial) phase when $\mu < |t|$ ($\mu > |t|$). The spectra of D_+ for two distinct DW configurations, created via spatial variation of μ, are reported in Fig. 2. As expected, there are midgap resonant modes trapped at the interfaces between the topological and trivial phases, which are always present regardless of the particular monotonic profile of the DWs [32]. Further spatial modulations of the parameter μ will result in more domain walls while maintaining the PH symmetry at all times, hence one can nucleate an arbitrarily large number of spatially localized modes, whose pulsations are all pinned at ω_0. Furthermore, by slowly changing the profile of μ, we can coherently displace the topological modes in space while keeping the pulsation pinned at ω_0. This supplies precise rules for how to modify the physical couplings and to ultimately implement this program in a laboratory [33], which is already unprecedented in a mechanical setting.

Fusion rules.—For our classical system, there are two distinct ways of creating the DWs, by interpolating μ between 0 and $\pm 2t$ as already exemplified in Fig. 2. We think of these two possibilities as the manifestation of a nontrivial internal structure of same excitation σ because both cases yield an identical energy spectrum. Furthermore, these two DW configurations can be both deformed into the topological-vacuum interface zero mode without breaking the PH symmetry or closing the bulk gap, e.g., by pushing the DWs to ends of the Kitaev chain.

In Fig. 3(a), we report the spectral flow as two σ excitations are adiabatically brought on top of each other via the $++$ channel. As one can see, the energies of the modes peel off from the midgap value and, when fused, the modes are completely lost to the bulk. Quite opposite, if the σ excitations are fused in the $(+-)$ channel as in Fig. 3(b), the modes persist and remain pinned in the middle of the gap. We have verified that this phenomena is not related to particular profiles of the domain walls and found that the rule is robust as long as the DWs are sufficiently smooth. We think of the result of $+-$ fusion as

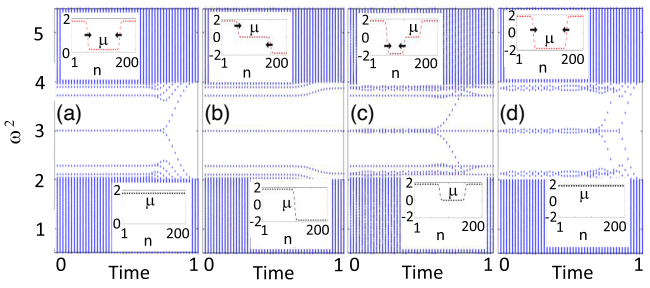

FIG. 3. The fusion results for different DW configurations, with insets indicating the configuration before and after the fusion: (a) $\sigma \times \sigma = 0$, (b) $\sigma \times \sigma = \psi$, (c) $\sigma \times \psi = \sigma$, and (d) $\psi \times \psi = 0$.

a new type of excitation ψ. The remaining fusion rules are computed in Figs. 3(c) and 3(d) and they match perfectly the ones for $SU(2)_2$ [34]: $\sigma \times \sigma = 0 + \psi$, $\sigma \times \psi = \sigma$, and $\psi \times \psi = 0$. These fusion rules are enabled by the ability to control the DW configurations of our classical system.

To explain the significance of 0, σ and ψ sectors and their fusion, we refer to Fig. 4, which shows two topological chains with sharp edges supporting topological midgap modes. These modes can be braided only if the interface supporting them is smooth, otherwise the interface cannot be displaced in an adiabatic fashion (the Hamiltonian will display jumps no matter how slow the displacement). The smoothing process can land the system in different DW configurations, as shown in Figs. 4(b) and 4(c). These configurations always fall either in 0 or ψ sectors (and σ if the number of DWs is odd). To determine the sector, one can simply collapse all DWs on top of each other to find one of the three possible outcomes, 0, σ, or ψ. Furthermore, the braidings can be implemented entirely in a single sector and we will give enough evidence that the braids depend in a nontrivial way on the DW configurations. Lastly, when more strands like the ones in Fig. 4(a) are added to the system, several distinct representations of the braid group can result, depending how the new strands are fused. The fusion rules supply a bookkeeping of these representations, in a manner which is yet to be determined.

Braiding the DW modes.—In our classical mechanics setup, the equation of motion is quadratic in time, $-\partial_t^2 \boldsymbol{Q} = D(t)\boldsymbol{Q}$. Nevertheless, the adiabatic theorem [23] still applies [22], more precisely, if the system is excited in any linear combination $\boldsymbol{Q}_{\omega_0}$ of midgap states, then at the end of the adiabatic cycle $\gamma(\tau)$ the system will oscillate as

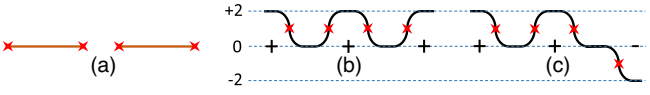

FIG. 4. (a) Two topological chains with sharp edges supporting midgap modes. (b),(c) Smoothing of the interfaces results in different spatial profiles of μ, labeled as $(+++)/(++-)$, and the system lands in the $0/\psi$ sectors, respectively.

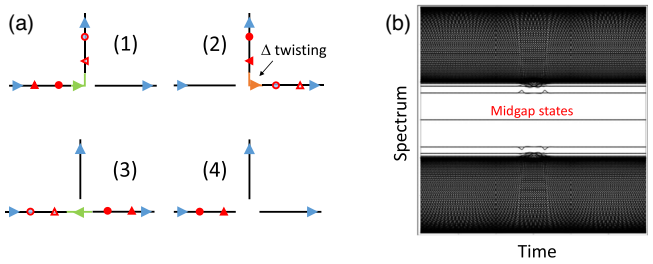

FIG. 5. (a). The T-junction braiding process, consisting of rigid slides of the DWs along the wires and adiabatic couplings/decouplings of the wires (shown as green/orange segments). The closed (open) circles and triangles denote the initial (final) positions of the DWs after each step in the braiding process, while the arrows indicate the direction of the coupling. The coupling at step (2) requires a special twist of the Δ parameter, denoted by the orange connection. (b) Evolution of the spectrum during the full T-junction process, demonstrating that the midgap states remain spectrally separated at all times.

$$\boldsymbol{Q}(t) = \mathrm{Re}[e^{\imath\omega_0 t} W_\gamma \boldsymbol{Q}_{\omega_0}], \tag{6}$$

where W_γ depends entirely on path γ inside the parameter space and can be conveniently computed as [25]

$$W_\gamma = \lim_{n\to\infty} P_{\gamma(\tau_n)} P_{\gamma(\tau_{n-1})} \ldots P_{\gamma(\tau_0)}, \tag{7}$$

where $\{\gamma(\tau_i)\}$ is a discretization of γ and $P_{\gamma(\tau)}$ is the projection onto the midgap spectrum at the moment τ.

The braidings will be performed through different fusion channels, using all the available DW configurations and, as we shall see, this will result in different outcomes. We first must make sure that our adiabatic braiding cycles are closed, i.e., $H_+(t_{\mathrm{init}}) = H_+(t_{\mathrm{final}})$ and that the bases we use are the same. For this, we always start/end our adiabatic cycles from a configuration where the zero modes are located at the clean ends of a chain and then we nucleate the desired smooth DW configurations. As for the adiabatic cycle, we employ the standard T-junction process illustrated in Fig. 5(a) [18] but with one important difference. Note that H_+ is not symmetric under the inversion operation $\mathcal{K}$, $\mathcal{K}H_+(\Delta)\mathcal{K}^{-1} = H_+(-\Delta)$. Hence, the chains come with a definite orientation, shown by the blue arrow in Fig. 5(a). If one insists on closing the braid cycle, then inherently two of the chains need to be fused in the wrong order, as it happens at step (2) in Fig. 5(a). Therefore, we are forced to connect two chains with opposite order parameters and, in order to keep the bulk gap open, that connection requires a rotation in the complex plane of the order parameter Δ. The precise expressions of the T-junction Hamiltonian is supplied in [22]. Figure 5(b) reports the evolution of the spectrum of this adiabatic Hamiltonian during the whole T-junction cycle, demonstrating that the midgap states are spectrally separated at all times.

We now demonstrate the topological character of the braids and consider the case of two DWs. If the DWs are well separated, then the space of midgap modes accepts a very special basis $\{\Psi_1, \Psi_2\}$, with Ψ_i's real valued and localized on one of the DWs. Independent of the location of the DWs in the T-junction geometry, such basis can be canonically generated. After an adiabatic exchange $1 \leftrightarrow 2$, the one-dimensional spaces corresponding to $\Psi_{1,2}$ are swapped and, since the basis remains real at all times, the exchange matrix U_{12} written in this basis takes an off diagonal form with real entries λ_{12} and λ_{21} and unitarity requires $\lambda_{12}^2 = \lambda_{21}^2 = 1$. This results in the possibilities $U_{12} = \pm\sigma_1$ or $\pm\imath\sigma_2$ hence, the monodromies are locked into one of these choices and continuous deformations cannot unlock them, hence the topological character.

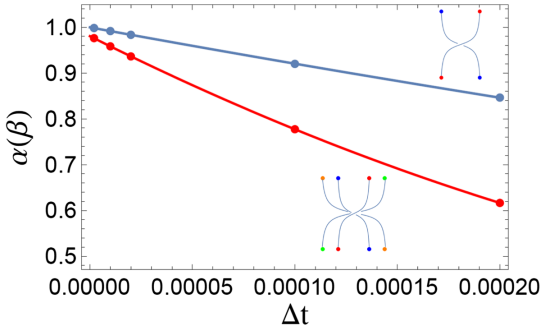

FIG. 6. Numerical evaluation of the braid cycles indicated in the diagram, as computed with (7). The graph reports $\alpha(\beta)$ (see text for definitions), which are plotted as a function of the adiabatic type step.

The evaluation of the braid matrix was performed using the T-junction geometry and Eq. (7) for the two braids shown in Fig. 6 via different DW configurations. The two midgap mode braid matrix via the $(++)$ channel can be expressed as $\alpha(\Delta t)[\imath\sigma_2]$, where $\alpha(\Delta\tau)$ plotted in Fig. 6 as a function of discretization step $\Delta\tau \to 0$. The fit to the scaling function, plotted in blue in Fig. 6, gives $\alpha(0) = 0.99978$, virtually converging to 1. Via the $(--)$ channel, we find that α converges to -1. For the other more complicated braids in Fig. 6, we found the braid matrix to be given by $\beta(\Delta t)[\imath\sigma_2 \otimes \sigma_2]$ in the $(+++)$ channel and $-\beta(\Delta\tau)[\sigma_1 \otimes \sigma_1]$ in the $(+-+)$ channel, where $\beta(\Delta\tau)$ is plotted in red in Fig. 6, with $\beta(\Delta\tau \to 0) = 0.98054$.

In a laboratory, for a pair of DWs, the two midgap modes can be loaded with arbitrary amplitudes and phases, leading to a collective oscillating state $\Psi(t) = \mathrm{Re}[\sum_{j=1,2} A_j \Psi_j e^{\imath(\omega_0 t + \phi_j)}]$. If one initiates two identical systems in the same load configuration, then one system can be braided while the other can be left untouched. After the exchange, the resonators will oscillate as

$$\Psi'(t) = \begin{cases} \mathrm{Re}(A_2\Psi_2 e^{\imath\phi_2} - A_1\Psi_1 e^{\imath\phi_1}) e^{\imath\omega_0 t} & (++\,\mathrm{ch}) \\ \mathrm{Re}(A_1\Psi_1 e^{\imath\phi_1} - A_2\Psi_2 e^{\imath\phi_2}) e^{\imath\omega_0 t} & (--\,\mathrm{ch}) \end{cases} \tag{8}$$

which can be directly compared with $\Psi(t)$ using the second system. In particular, the emergence of the geometrical and topological phase of π can be probed.

In conclusion, we have supplied a classical analog of a fully general topological chain from class D, where all accidental symmetries are broken and the complex superconducting parameter Δ as well as the chemical potential μ can be manipulated by changing the coupling strengths between the resonators. This enabled us to create DWs supporting topological midgap states and to implement several braidings using T junctions. We discovered that the braid matrices depend on the DWs configurations, which fall into three sectors displaying fusion rules similar to those for $SU(2)_2$. The braiding structure turned out to be far more interesting than anyone anticipated and this could be a proof that topological metamaterials could find applications in information processing.

Both authors acknowledge financial support from the W. M. Keck Foundation. Y. B. acknowledges additional support from UNR/VPRI start-up grant and E. P. from NSF Grant No. DMR-1823800.

[1] Z. Wang, Y. Chong, J. D. Joannopoulos, and M. Soljacic, Observation of unidirectional backscattering-immune topological electromagnetic states, Nature (London) **461**, 772 (2009).
[2] M. Hafezi, S. Mittal, J. Fan, A. Migdall, and J. M. Taylor, Imaging topological edge states in silicon photonics, Nat. Photonics **7**, 1001 (2013).
[3] L.-H. Wu and X. Hu, Scheme for Achieving a Topological Photonic Crystal by Using Dielectric Material, Phys. Rev. Lett. **114**, 223901 (2015).
[4] E. Prodan and C. Prodan, Topological Phonon Modes and Their Role in Dynamic Instability of Microtubules, Phys. Rev. Lett. **103**, 248101 (2009).
[5] S. H. Mousavi, A. B. Khanikaev, and Z. Wang, Topologically protected elastic waves in phononic metamaterials, Nat. Commun. **6**, 8682 (2015).
[6] R. Chaunsali, C.-W. Chen, and J. Yang, Subwavelength and directional control of flexural waves in zone-folding induced topological plates, Phys. Rev. B **97**, 054307 (2018).
[7] C. L. Kane and T. C. Lubensky, Topological boundary modes in isostatic lattices, Nat. Phys. **10**, 39 (2014).
[8] L. M. Nash, D. Kleckner, A. Read, V. Vitelli, A. M. Turner, and W. T. M. Irvine, Topological mechanics of gyroscopic metamaterials, Proc. Natl. Acad. Sci. U.S.A. **112**, 14495 (2015).
[9] R. Süsstrunk and S. D. Huber, Observation of phononic helical edge states in a mechanical topological insulator, Science **349**, 47 (2015).
[10] J. Paulose, B. G. -g. Chen, and V. Vitelli, Topological modes bound to dislocations in mechanical metamaterials, Nat. Phys. **11**, 153 (2015).
[11] E. Prodan, K. Dobiszewski, A. Kanwal, J. Palmieri, and C. Prodan, Dynamical Majorana edge modes in a broad class of topological mechanical systems, Nat. Commun. **8**, 14587 (2017).
[12] A. P. Schnyder, S. Ryu, A. Furusaki, and A. W. W. Ludwig, Classification of topological insulators and superconductors in three spatial dimensions, Phys. Rev. B **78**, 195125 (2008).
[13] X.-L. Qi, T. L. Hughes, and S.-C. Zhang, Topological field theory of time-reversal invariant insulators, Phys. Rev. B **78**, 195424 (2008).
[14] A. Kitaev, Periodic table for topological insulators and superconductors (Advances in Theoretical Physics: Landau Memorial Conference), AIP Conf. Proc. **1134**, 22 (2009).
[15] S. Ryu, A. P. Schnyder, A. Furusaki, and A. W. W. Ludwig, Topological insulators and superconductors: Tenfold way and dimensional hierarchy, New J. Phys. **12**, 065010 (2010).
[16] A. Y. Kitaev, Unpaired Majorana fermions in quantum wires, Phys. Usp. **44**, 131 (2001).
[17] L. Fu and C. L. Kane, Superconducting Proximity Effect and Majorana Fermions at the Surface of a Topological Insulator, Phys. Rev. Lett. **100**, 096407 (2008).
[18] J. Alicea, Y. Oreg, G. Refael, F. v. Oppen, and M. P. A. Fisher, Non-Abelian statistics and topological quantum information processing in 1D wire networks, Nat. Phys. **7**, 412 (2011).
[19] V. Mourik, K. Zuo, S. M. Frolov, S. R. Plissard, E. P. a. M. Bakkers, and L. P. Kouwenhoven, Signatures of Majorana fermions in hybrid superconductor-semiconductor nanowire devices, Science **336**, 1003 (2012).
[20] Y. Barlas and E. Prodan, Topological classification table implemented with classical passive metamaterials, Phys. Rev. B **98**, 094310 (2018).
[21] D. J. Apigo, K. Qian, C. Prodan, and E. Prodan, Topological edge modes by smart patterning, Phys. Rev. Mater. **2**, 124203 (2018).
[22] See Supplemental Material at http://link.aps.org/supplemental/10.1103/PhysRevLett.124.146801, which includes Refs. [23,24], for the degeneracy counting argument, braid group representations, and formulation of the classical adiabatic theorem.
[23] T. Kato, On the adiabatic theorem of quantum mechanics, J. Phys. Soc. Jpn. **5**, 435 (1950).
[24] F. Wilczek and A. Zee, Appearance of Gauge Structure in Simple Dynamical Systems, Phys. Rev. Lett. **52**, 2111 (1984).
[25] E. Prodan and F. D. M. Haldane, Mapping the braiding properties of the Moore-Read state, Phys. Rev. B **80**, 115121 (2009).
[26] P. Boross, J. K. Asboth, G. Szechenyi, L. Oroszlany, and A. Paly, Poor man's topological quantum gate based on the Su-Schrieffer-Heeger model, Phys. Rev. B **100**, 045414 (2019).
[27] T. Iadecola, T. Schuster, and C. Chamon, Non-Abelian Braiding of Light, Phys. Rev. Lett. **117**, 073901 (2016).
[28] L. S. Simeonov and N. V. Vitanov, Generation of non-Abelian geometric phases in degenerate atomic transitions, Phys. Rev. A **96**, 032102 (2017).
[29] A practical procedure for how to accomplish just that is supplied in Ref. [20].
[30] It is well established that the s-wave superconductivity in the presence of spin-orbit coupling, results in an effective p-wave superconductor.
[31] With passive metamaterials, it is impossible to simulate a single Kitaev chain.

[32] To implement smooth adiabatic processes, the DW profiles need to be rounded, *e.g.,* as $\delta\mu\{(1+\tanh[(x-x_{\mathrm{DW}})/\ell]\}$, where x_{DW} is the center of the wall, ℓ is the width of the wall and $\delta\mu$ is the full variation of μ.

[33] Ref. [20] explains in details how derive the physical couplings from a Hamiltonian written as in Eqs. (2) and (3).

[34] Z. Wang, *Topological Quantum Computation* (AMS, Providence, 2010).